Scilight

Bulletin of Computational Intelligence
https://www.sciltp.com/journals/bci



Article

Check for updates

A Unified Physics Informed Data Driven Framework for Residual Shear Strength Prediction in Indian Coarse-Grained Soils

Shubhendu Vikram Singh [1,*], Sufyan Ghani [2] and Faizanul Haque [1]

[1] Department of Civil Engineering, Sharda University, Noida 201310, Uttar Pradesh, India
[2] WSP Consultants India Private Limited, Noida 201301, Uttar Pradesh, India
* Correspondence: 2022453567.shubhendu@dr.sharda.ac.in

How To Cite: Singh, S.V.; Ghani, S.; Haque, F. A Unified Physics Informed Data Driven Framework for Residual Shear Strength Prediction in Indian Coarse-Grained Soils. *Bulletin of Computational Intelligence* **2026**, *2*(4), 362–385. https://doi.org/10.53941/bci.2026.100019

Received: 10 August 2026
Revised: 29 October 2026
Accepted: 5 November 2026
Published: 25 November 2026

Abstract: Accurate estimation of residual shear strength (S_{ur}) of coarse-grained soils is essential for post-failure and post-liquefaction stability assessment but it is limited to scarcity laboratory data and field measurements. This study presents a physics informed data driven framework integrating Direct Shear (DST), Reverse Direct Shear (R-DST), Multivariate Normal (MVN) augmentation, DCPT calibration, and Multiple Linear Regression (MLR) for S_{ur} prediction. Four interpretable strength-degradation indicators as strength loss (Δ), strength-retention ratio (R), brittleness index (I_b), and post-peak energy index (E) were derived from the laboratory response. MVN sampling with Cholesky covariance preservation was used to expand the experimental database, followed by geotechnical admissibility screening. The DCPT calibration achieved R^2 = 0.972 with an independent MAE of 2.5 blows (4.8%). Material-specific MLR models achieved R^2 = 0.941 for sand and 0.932 for gravel, with d_{50} additionally incorporated for gravel. Monte Carlo simulation with 10,000 realizations quantified prediction uncertainty, and the validated framework was subsequently applied to representative regional conditions for state-wise S_{ur} zonation across India. The proposed framework integrates post-peak characterization, physics-informed data augmentation, and field-oriented prediction into a transparent computational approach for estimating S_{ur} from measurable geotechnical parameters.

Keywords: residual shear strength (S_{ur}); multivariate normal distribution (MVN); cholesky decomposition; dynamic cone penetration test (DCPT); multivariate regression (MVR); geotechnical computing

1. Introduction

The strength involved in geotechnical studies related to liquefaction is made up of several parameters related to the state of the soil, drainage, loading conditions, and deformation modes [1–3]. They include the peak shear strength (S_p), S_{ur}, strength ratios, and cyclic resistance parameters [2,4–6]. Although similar in nature, these different parameters must be understood to make predictions related to liquefaction behavior [2,7].

The S_p denotes the maximum shear strength mobilized prior to post-peak softening while the S_{ur} denotes the strength mobilized at large deformations after significant strain softening, and pore-pressure generation in case of applications involving liquefaction [2,4,8]. The residual strength is an important consideration in the analysis of flow failure and lateral spreading [2,4,6,9–11]. There are correlations that have been used in the estimation of the residual strength, and they include those based on experience from real-world cases [4,6,9,12,13] and those based on penetration resistance, and these are from Standard Penetration Test (SPT) [7,13,14], Cone Penetration Test

Copyright: © 2026 by the authors. This is an open access article under the terms and conditions of the Creative Commons Attribution (CC BY) license (https://creativecommons.org/licenses/by/4.0/).
Publisher's Note: Scilight stays neutral with regard to jurisdictional claims in published maps and institutional affiliations.

(CPT) [6,7,15,16], Dynamic Cone Penetration Test (DCPT) [17,18], and shear wave velocity measurements [19]. Alongside field correlations, laboratory experiments have played an essential role in characterizing the large-strain behavior of soils through monotonic and cyclic triaxial tests [3,5,20], centrifuge modeling [21], direct shear tests (DST) [22–24], and ring shear tests (RST) [25], while rheological and constitutive frameworks have further explored post-liquefaction deformation mechanisms [26,27]. Steady-state theory provides a foundational framework for analyzing the large-strain behavior of contractive soils [2,4], although steady-state strength and field residual strength may not always be identical due to drainage, void redistribution, and fabric effects [5,8,25].

Normalized strength ratios like liquefied strength/initial vertical effective stress enable comparisons among stress states and form the backbone for empirical relations based on flow failure experience [6–8,13,28]. This is separate from the Cyclic Resistance Ratio (CRR), which measures resistance to the earthquake-induced liquefaction triggering, and Factor of Safety, which expresses the relationship between resistance and demand of triggering [14,15,29,30]. Conventional procedures that were devised by [2,15,29,31] form the basis of the conventional triggering evaluation process. Post-liquefaction deformation assessment, on the other hand, might need residual-strength properties for the estimation of lateral spreading, settlement, or flow deformation [10,11,27]. Liquefaction behavior and cyclic resistance studies from India include Brahmaputra sand and liquefaction hazard in Kolkata [20,30,32].

The performance and behavior of granular soils are influenced by various parameters, such as particle-size distribution, fines content, relative density, fabric of soil, saturation level, stress history, and test parameters [3,33–38]. The study of sand-silt mixtures has shown that fines content may affect the behavior of the soil before and after liquefaction [34,38]. Tests conducted for natural sands, tailings, and other geomaterials serve as more examples of application of strength concepts to these materials [5,12,20,32,39]. However, results obtained for various geomaterials and by various testing techniques need proper evaluation to be used for estimation of residual strength of soils [4,8,26,28]. Some relevant testing techniques include monotonic and cyclic triaxial tests, DST, RST, and tests based on determination of penetration resistance [3,5,7,15–19,21–25]. Additional investigations have been conducted to analyse the effect of soil conditioning and properties of materials on the behavior of shear strength and application of prediction techniques based on data [11,17,18,40]. Ref. [41] studied the effect of soil moisture content, relative density, vertical stress, and polypropylene fibers on poorly graded sandy soil, while [42] reviewed the technique of artificial intelligence used to predict strength properties of waste-stabilized soils. However, none of these investigations validate relationships of residual shear strength of liquefied soils.

In spite of developments in laboratory experiments, empirical relationships, and data-driven modeling techniques, prediction of residual shear strength is still difficult owing to the dependence of soil properties on the interaction of geotechnical factors and access to appropriate experimental data [1,8,9,28,37]. Thus, a need for interpretability and physically informed prediction models tailored for the investigated soil emerges. The current research develops a unified physics-informed and data-driven methodology for prediction of residual shear strength in Indian coarse-grained soils in respect of the soils containing mainly sand and gravel, respectively [23,35,36,43]. The methodology utilizes MVN augmentation, geotechnical constraints selection, and MLR analysis, which is then assessed for statistical, predictive, and reliability performance.

It is known from past experimental investigations that the shear properties of granular materials are not solely a function of stress-state and density but also of the grain size distribution and the materials composition [24,33,38]. Ref. [44] showed that grain-size ratio affects the shear strength, dilation and compressibility of sand-rubber composites, and ref. [33] found differences in the friction and dilation angles with the median grain size of poorly-graded sands. These results justify physically the use of grain size and gradation features in the understanding of the shear strength properties of granular materials. Nonetheless, the importance of any one feature in this empirical equation depends upon whether or not the feature is available in the data set and included in the regression.

2. Research Gap, Objectives and Significance

Even after extensive research conducted on liquefaction and post-peak soil behavior, it is difficult to estimate the S_{ur} of coarse-grained soils. Current methods mainly concentrate on peak and residual strength but give little importance to the quantification of the post-peak behavior of soils. In addition, even though SPT and CPT correlations are extensively used, the possibility of DCPT for estimating residual strength needs to be explored more. The regional variation of S_{ur} also needs attention considering the different types of soils in India.

For these problems, this paper proposes a study on post-peak shear response through DST and R-DST, and assessment of four parameters that describe strength degradation behavior: Δ, R, I_b, and E. The paper also suggests an empirical model for estimation of S_{ur} of coarse-grained soils based on certain geotechnical parameters, DCPT-

derived data, and MVN data augmentation constrained by physical limits. These models are assessed through statistics, whereas prediction uncertainty analysis is done through Monte Carlo simulation under given assumptions.

Lastly, the obtained relationships are used for the analysis of regional soil conditions to develop an initial residual strength zonation map for India on a state-by-state basis. The main purpose of the work is to create a comprehensible field approach for the preliminary geotechnical assessment. The practical value of the suggested relationships depends on the diversity and quality of data used and needs to be validated before application in other geological areas.

3. Experimental Program and Data Collection

3.1. Soil Collection, Classification, and Particle Size Distribution Analysis

Representative coarse-grained soils spanning the SP, SW, SM, SC, GP, and GW classes (IS: 1498) were collected from multiple project locations and used to establish the S_{ur} database for this study. For the detailed laboratory program, a parent sand typical of the Indo-Gangetic alluvium was selected as the reference material because of its widespread use in embankments, foundations, backfills, and subgrade systems. This material formed the baseline for controlled variations in relative density (D_r), fines content, and degree of saturation (S_r) required for the Direct Shear Test DST, R-DST, and subsequent S_{ur} modelling.

To characterize the fundamental gradation properties, washed sieve analysis was performed according to IS 2720 using three specimens (S1–S3) to assess variability in the parent sand. The resulting particle-size distribution (PSD) curves, plotted on a semi-logarithmic scale (Figure 1a–d), show similar gradation profiles. The characteristic particle sizes are D_{10} = 0.086–0.11 mm, D_{30} = 0.220–0.225 mm, and D_{60} = 0.421–0.539 mm. The corresponding coefficients of uniformity (C_u) and curvature (C_c) are summarized in Table 1. Based on the reported gradation coefficients, the parent sand does not satisfy the IS 1498 criteria for well-graded sand (SW) and is therefore classified as poorly graded sand (SP), provided its fines content is below 5%.

The coefficients of uniformity and curvature were calculated using the standard relationships

$$C_u = \frac{D_{60}}{D_{10}},\ C_c = \frac{(D_{30})^2}{D_{60}D_{10}} \tag{1}$$

The individual samples have C_u values of 4.70–5.32 and C_c values of approximately 0.89–1.34. These values do not satisfy both IS 1498 criteria for well-graded sand (SW); therefore, the parent sand is treated as poorly graded sand (SP), subject to confirmation that its fines content is below 5%.

Using a common parent sand provides a consistent baseline for the experiments, while the deliberate variation in fines content modifies the gradation of the prepared mixtures. Accordingly, the observed strength changes are interpreted in relation to the specified test conditions and mixture composition.

- Relative Density: Loose ($D_r \approx$ 30–35%), Medium dense ($D_r \approx$ 40–55%), Dense ($D_r \approx$ 70–80%) and Very Dense ($D_r \approx$ 85%)
- Fines Content: 5%, 15%, and 25% passing 75 μm
- Degree of Saturation: Dry (S_r = 0%), Partially saturated ($S_r \approx$ 50%), and fully saturated (S_r = 100%)

Establishing this consistent baseline is critical for S_{ur} prediction, as residual strength in coarse-grained soils is governed by grain-scale mechanisms—such as contact sliding, fabric collapse, and post-peak particle realignment—that are themselves highly sensitive to PSD and gradation. Performing DST and R-DST on a well-characterized parent sand and its prepared mixtures enables interpretation of strength degradation under the investigated conditions and supports the development of the field-scale DCPT-derived S_{ur} model presented later in this study.

Table 1. Characteristic grain-size parameters (D_{10}, D_{30}, D_{60}) and gradation coefficients (C_u, C_c) for coarse sand samples (S1–S3) and combined average.

Sample	D_{10} (mm)	D_{30} (mm)	D_{60} (mm)	C_u	C_c
S1	0.11	0.225	0.518	4.7	0.89
S2	0.101	0.221	0.539	5.34	0.9
S3	0.086	0.22	0.421	4.9	1.34
Combined (avg)	0.099	0.222	0.493	4.98	1.04

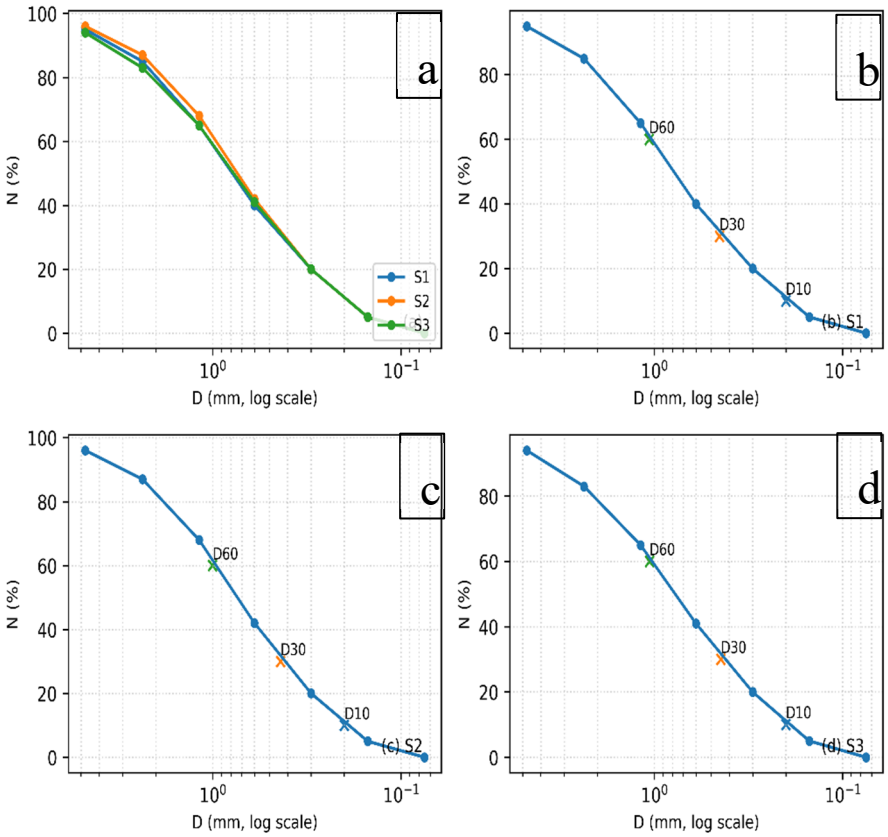

Figure 1. Particle size distribution (PSD) curves for coarse-grained sand. (**a**) Combined PSD of three representative samples (S1–S3). (**b**–**d**) Individual PSDs with characteristic grain sizes (D_{10}, D_{30}, D_{60}) marked.

3.2. Laboratory Testing Overview

A comprehensive laboratory program was conducted to evaluate the shear behaviour of coarse-grained soils and to generate a high-quality database for S_p, S_{ur} and degradation indices. The experimental work focused on six controlled variables essential for S_{ur} prediction: relative density, fines content, degree of saturation, forward shearing, reverse shearing, and field laboratory consistency through DCPT.

3.2.1. Direct and Reverse Direct Shear Testing—Experimental Setup

The shear testing was performed on a motorized direct shear apparatus (HEICO HS24 series) was manufactured by Hydraulic & Engineering Instruments (HEICO), Sonipat, Haryana, India., conforming to IS: 2720 (Part 13) [23] and BS 1377 (Part 7) [22] (Figure 2a). The machine comprises a 60 mm × 60 mm split shear box, horizontal and vertical LVDTs for displacement measurement, a motorized loading system, and a digital control panel for strain-rate regulation. The arrangement ensures fully drained shearing, essential for characterizing coarse-grained soil behaviour.

The shear box assembly, including clamping bolts, grid plates, and loading pads (Figure 2b), provides uniform load transfer and prevents slippage during forward and reverse shearing. Tests were conducted under normal stresses of 49, 98, and 147 kPa, representing stress levels typical of foundations, retaining structures, and shallow slopes.

The forward shearing was done first in order to get the S_p from the $(\tau - \delta)$ curve and was extended even after the peak in order to observe the softening of the material beyond the peak. No disturbance was done on the material and σ_n was kept constant while doing one reversal of horizontal displacement in the same shear plane. The resulting large displacement shear resistance was considered as the experimental S_{ur} in the current test setup. But only one reversal was done and no plateau criterion or acceptable strength variability was set for the residual state.

The S_{ur} obtained from the present laboratory DST programme represents the shear resistance measured at large displacement under the adopted testing and drainage conditions. It should not be considered directly equivalent to the undrained residual strength mobilized in liquefied soils, which depends on pore-pressure generation, drainage conditions, and the stress path. Accordingly, the empirical relationships developed in this study are intended to predict the residual shear strength represented by the laboratory dataset. Their application to

post-liquefaction undrained strength assessment requires further validation using appropriate undrained testing, including pore-pressure measurements.

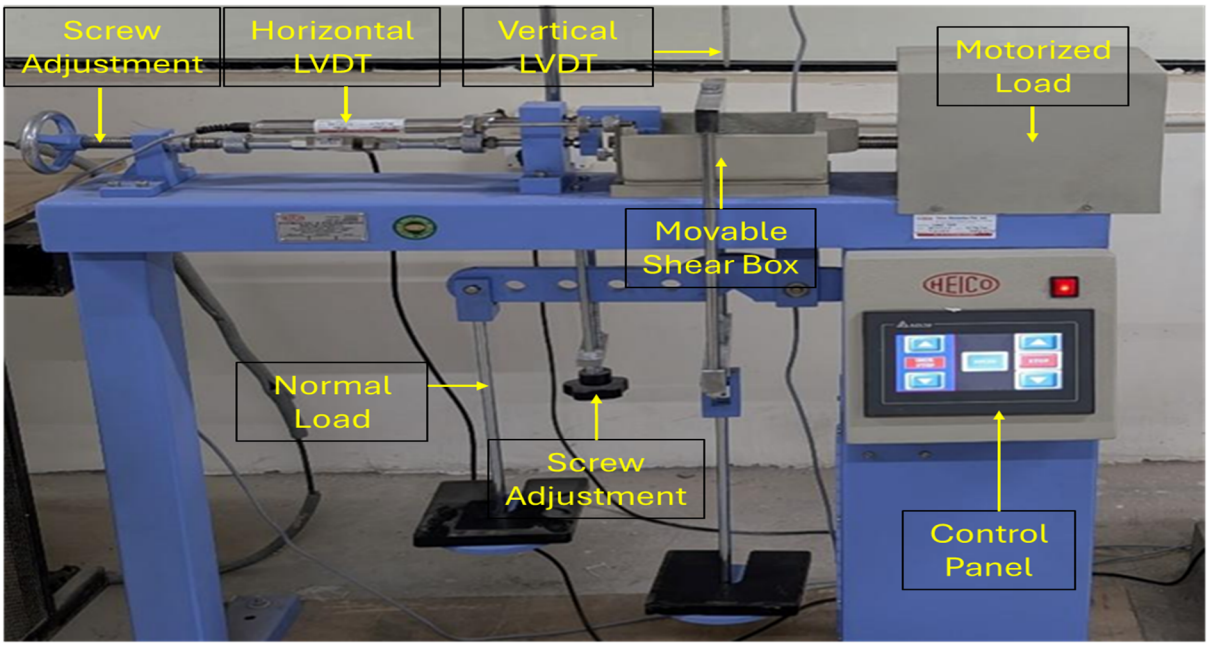

(**a**)

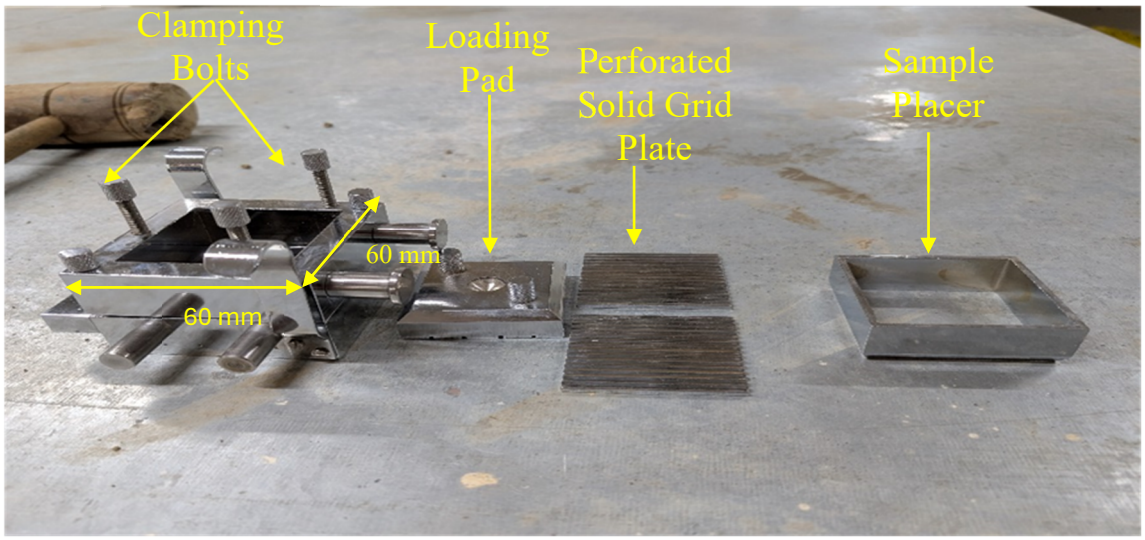

(**b**)

Figure 2. (**a**) Motorized direct shear test apparatus with lever loading system and digital indicator. (**b**) Split shear box showing porous stones and loading plate.

3.2.2. Determination of Relative Density (D_r)

D_r was adopted as a key control parameter because peak strength, dilatancy, and residual behaviour of sands are strongly governed by density state. Maximum and minimum dry densities (γ_{dmax}, γ_{dmin}) were determined following IS: 2720 (Part 14) [35] using the standard mould, surcharge weight, collar, dial gauge, and vibrating table (Figure 3a). Relative density was computed using either void ratio or density form:



(**a**)



(**b**)

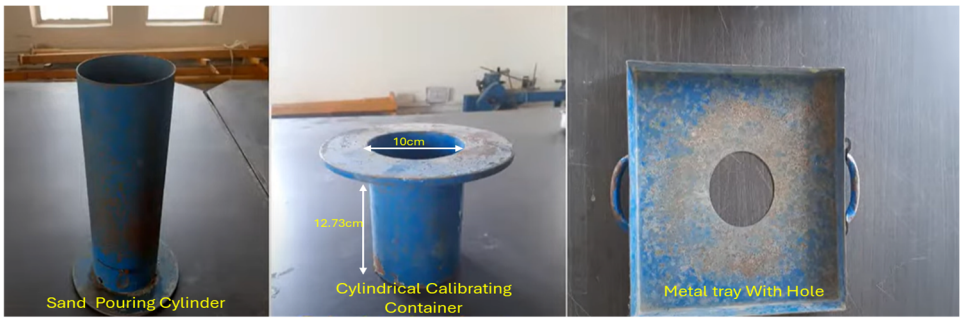

(**c**)

Figure 3. (**a**) Apparatus for determination of relative density of cohesionless soil. (**b**) Prepared soil specimens at loose ($D_r \approx 35\%$) and dense ($D_r \approx 75\%$) states. (**c**) Apparatus for sand replacement method. (**left**) Sand pouring cylinder, (**middle**) cylindrical calibrating container, and (**right**) metal tray with central hole.

$$D_r = \frac{e_{max} - e}{e_{max} - e_{min}} \text{ or } D_r = \frac{\gamma_d - \gamma_{dmin}}{\gamma_{dmax} - \gamma_{dmin}} \tag{2}$$

Representative loose ($D_r = 35\%$) and dense ($D_r = 75\%$) specimens are shown in Figure 3b. Field verification of density used the Sand Replacement Method (IS: 2720 Part 28) with the pouring cylinder, calibrating container, and tray (Figure 3c). Bulk and dry densities were obtained from.

$$\gamma_{bulk} = \frac{W_{wet}}{V_h} \gamma_d = \frac{\gamma_{bulk}}{1 + w} \tag{3}$$

3.2.3. Fines Content (5–25% Passing 75 μm)

To quantify the influence of fines on S_p and S_{ur}, controlled fines levels of 5% (in gravel) and 15% and 25% (in clean sand) were introduced into clean sand following IS: 2720 (Part 13) [23]. The fines fraction (<75 μm) was separately collected, oven-dried, and re-blended with sand in precise proportions. These levels represent are as 5% of clean to slightly silty sand, 15% transition fines beginning to fill voids, 25% fines-dominated mixture

approaching silty sand. Specimens were prepared at loose and dense states using pluviation and vibration, respectively. Representative mixtures are shown in Figure 4.



Figure 4. Sand–fines mixtures containing 5%, 15%, and 25% fines.

3.2.4. Degree of Saturation (S_r = 0–100%)

Three saturation states were selected to capture the influence of pore water on three states of samples Dry (S_r = 0%) oven-dry material placed directly in the shear box, partially saturated (S_r = 50%) achieved through controlled wetting drying cycles and fully saturated (S_r = 100%)—achieved through back-saturation with a small hydraulic head. The target water content for partial saturation was estimated using:

$$S_r = \frac{wG_s}{e},\ w_{target} = \frac{S_r e}{G_s} \tag{4}$$

Representative prepared specimens for dry, partially saturated, and saturated states are shown in Figure 5. Shear testing under these saturation levels provides insights into pore-water softening, fabric collapse, and the transition from dilative to contractive response, all of which are crucial for accurate S_{ur} modelling.

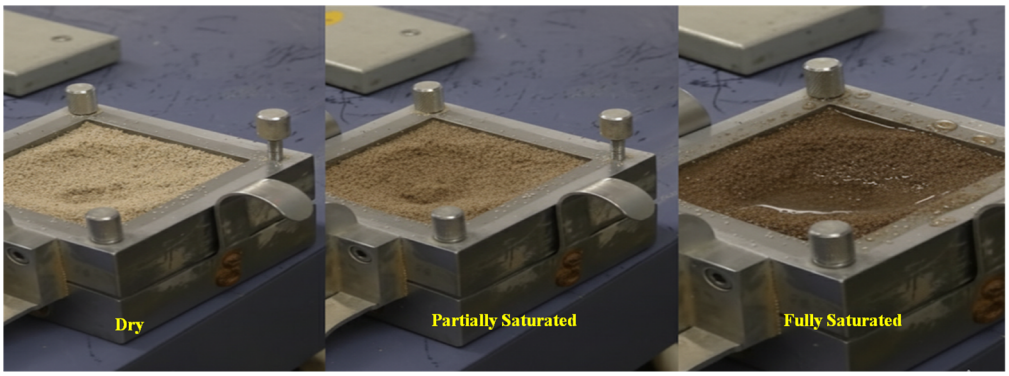

Figure 5. Samples prepared under dry, partially saturated, and fully saturated states.

3.2.5. Integration with Field Testing (DCPT)

To ensure that laboratory-derived S_{ur} values can be reliably translated to field conditions, Dynamic Cone Penetration Tests (DCPT) were conducted across selected project sites. The DCPT is widely used in India because of its portability, low cost, and ability to provide continuous resistance profiles in granular soils, making it a suitable candidate for residual strength estimation where SPT or CPT may not be feasible.

To ensure that laboratory-derived S_{ur} values can be reliably translated to field conditions, Dynamic Cone Penetration Tests (DCPT) were conducted across selected project sites. The DCPT is widely used in India because of its portability, low cost, and ability to provide continuous resistance profiles in granular soils, making it a suitable candidate for residual strength estimation where SPT or CPT may not be feasible. The field apparatus consisted of an 8 kg hammer, 20 mm diameter cone, and a 60° tip angle, operated using standard free-fall conditions (Figure 6). Penetration was recorded after each hammer blow, and the dynamic resistance was computed using:

$$q_d = \frac{(m + m')}{m} \cdot \frac{E}{Ae} \tag{5}$$

where m′ is rod/anvil mass, A is cone tip area, and e is penetration per blow.

Because Indian practice often requires compatibility with SPT-based design charts, the DCPT resistance was converted to an equivalent SPT blow count (N_{SPT}) using an empirical correlation. Equation (6) was used to estimate equivalent SPT blow counts from dynamic cone resistance. Refs. [16,28] demonstrated DCPT applications in geotechnical assessment and liquefaction analysis. However, the calibration range and uncertainty of this specific equation could not be verified; its applicability to the present coarse-grained soils should therefore be interpreted cautiously.

$$N_{SPT} = 5.76 q_d^{0.74} \quad (6)$$

This step enabled direct comparison with laboratory-determined S_{ur} and provided a basis for developing a DCPT-driven residual strength prediction model. Field data were then paired with laboratory S_{ur} from matched soil classifications (SP–SW–SM–SC), ensuring that the resulting model captures realistic behavior across Indian coarse-grained deposits.

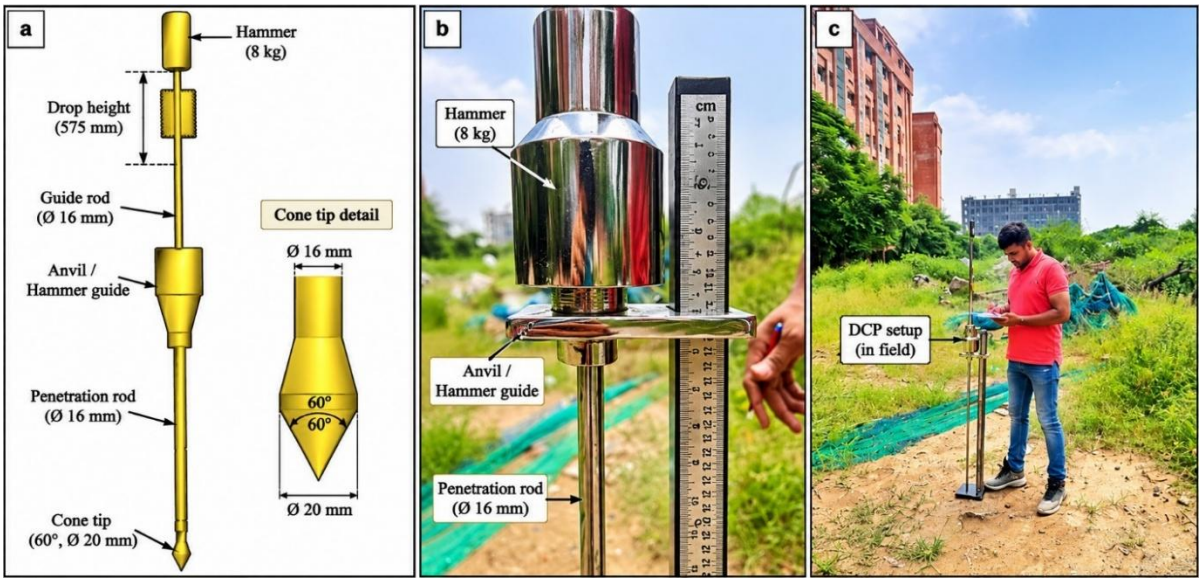

Figure 6. (**a**) DCPT schematic (cone, anvil, rods, hammer), (**b**) field rig close-up: Hammer, anvil, depth gauge, (**c**) *in-situ* test: Operator & setup.

4. Data Analysis and Interpretation

This section presents a structured interpretation of the laboratory shear test results by examining how peak strength, residual strength, and post-peak degradation evolve under controlled variations in relative density, fines content, and saturation. Using τ–δ response curves, computed degradation descriptors (Δ, R, I_b, E), and comparative visual analyses (Figures 7–14), the section identifies key behavioral trends that govern the transition from peak to residual strength in coarse-grained soils. Together, these analyses provide the mechanistic basis for understanding strength loss, brittleness, and energy dissipation—insights that are essential for developing the empirical S_{ur} prediction model and ensuring its physical reliability.

As R and I_b are mathematically related, they are interpreted as alternative representations rather than independent descriptors. The E is considered separately as an indicator of the energy-related response during shearing, according to its definition in this study.

4.1. Strength-Degradation Metrics: Definitions and Physical Meaning

S_{ur} does not merely represent the end point of a τ–δ curve also reflects a progressive degradation pathway controlled by interlocking, fines migration, dilation-contraction cycles, and saturation-mediated pore interaction. To quantify this transition, four degradation descriptors were formulated to simplify the understanding.

4.1.1. Strength Loss (Δ)

$$\Delta = S_p - S_{ur} \quad (7)$$

where S_p is the peak shear strength (kPa) and S_{ur} is the undrained/post-peak residual shear strength (kPa), yielding Δ in kPa. Δ represents the absolute drop in shear strength from peak to residual state. High Δ means

brittle collapse (typical in dense, dry sands), whereas low Δ means ductile sliding (typical in loose or fully saturated sands).

4.1.2. Strength Retention Ratio (R)

$$R = \frac{S_{ur}}{S_p} \tag{8}$$

R expresses how much of the peak strength is preserved at residual state. R = 1 means minimal degradation (ductile). Lower R means significant softening (brittle).

4.1.3. Brittleness Index (I_b)

$$I_b = \frac{S_p - S_{ur}}{S_p} = 1 - R \tag{9}$$

I_b directly measures brittleness. $I_b \approx 0.20$–0.30 means moderate brittleness, $I_b > 0.30$ means highly brittle post-peak behaviour.

4.1.4. Post-Peak Energy Index (E)

$$E = \Delta \times \sigma_n = [S_p - S_{ur}]\,\sigma_n \tag{10}$$

where $\Delta = S_p - S_{ur}$ is the post-peak shear strength drop (kPa) and σ_n is the applied normal stress (kPa), giving E in units of kPa^2. E provides a stress-weighted index of post-peak strength degradation from peak to residual. Higher E indicates greater particle rearrangement, dilation collapse, or grain crushing under higher confinement. Dense or partially saturated sands often show $E > 1500\ kPa^2$, marking a more destructive failure mechanism. Together, Δ, R, I_b, and E offer a mechanistic fingerprint of soil behaviour, enabling degradation trajectories to be interpreted rather than relying solely on S_p and S_{ur} values.

4.2. Representative τ–δ Behaviour under Varying Laboratory Conditions

Figure 7 presents τ–δ responses under three conditioning variables: (a) Relative density (D_r = 35% and 75%) (b) Fines content (5%, 15%, 25%) (c) Saturation (S_r = 0%, 50%, 100%). These curves capture how peak strength, residual strength and the shape of the post-peak branch evolve across the tested stress levels (49, 98, 147 kPa).

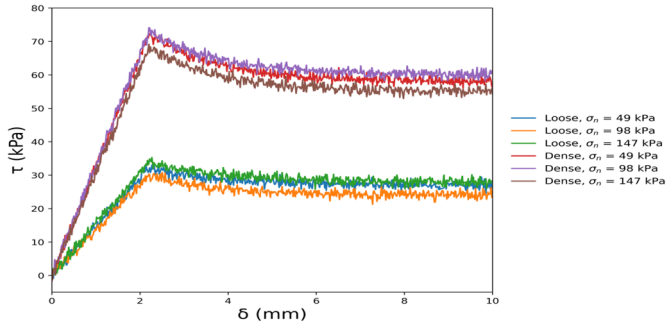

(**a**)

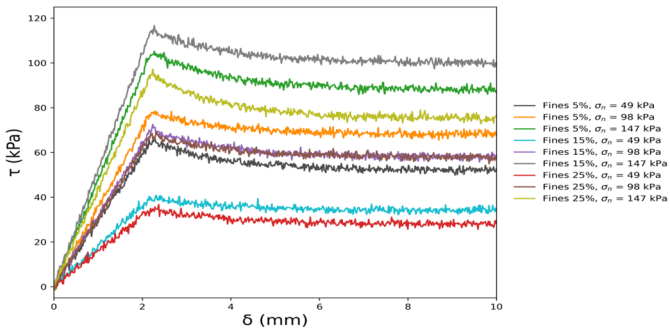

(**b**)

Figure 7. *Cont.*

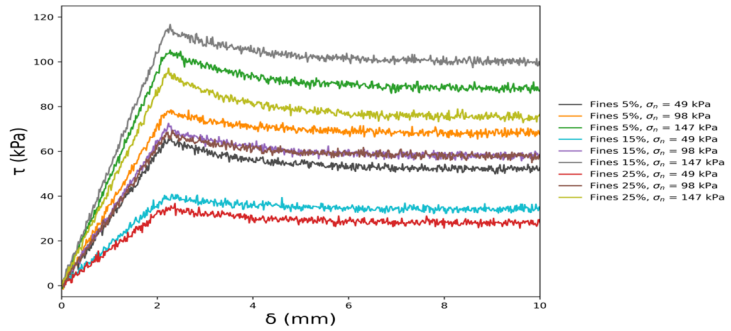

(**c**)

Figure 7. Representative τ–δ curves for coarse-grained soils at σ_n = 49, 98, 147 kPa under different laboratory conditions: (**a**) relative density (**b**) fines% (**c**) saturation.

4.3. Parametric Analysis of Shear Strength Behavior

4.3.1. Effect of Relative Density (D_r)

Dense sand (D_r = 75%) consistently mobilises far higher peak strength (S_p) than loose sand due to enhanced particle interlock and dilative resistance. At (σ_n = 98) kPa, the peak shear strengths reported in Table 2 are 75.2 kPa for dense sand and 62.6 kPa for loose sand. However, dense sands also experience significantly greater degradation Δ = 14–16 kPa (dense), Δ = 6–7 kPa (loose). Interestingly, R = 0.80 and I_b = 0.20 remain nearly constant across D_r levels suggesting that while the magnitude of degradation changes, the proportion of retained strength relative to peak capacity remains similar. This is in agreement with previous observations that have shown that relative density and vertical stress have an effect on shear strength of sandy soil [41]). The peak and post-peak strength trends discussed here are based on the present study; findings from other soils cannot, by themselves, establish the residual strength of the soils investigated here.

Table 2. Computed S_p, S_{ur}, Δ, R, I_b, and E for coarse-grained soils under varying relative density, fines content, and saturation.

Sr No	Soil Group	Condition	σ_n (kPa)	S_p (kPa)	S_{ur} (kPa)	Δ (kPa)	R	I_b	E
1	Sand	Loose state (D_r = 35%), dry	49	33.6	25.67	7.93	0.76	0.24	389
2	Sand	Loose state (D_r = 35%), dry	98	62.6	47.83	14.77	0.76	0.24	1448
3	Sand	Loose state (D_r = 35%), dry	147	91.6	69.98	21.62	0.76	0.24	3178
4	Sand	Dense state (D_r = 75%), dry	49	46.2	36.96	9.24	0.8	0.2	453
5	Sand	Dense state (D_r = 75%), dry	98	75.2	60.16	15.04	0.8	0.2	1474
6	Sand	Dense state (D_r = 75%), dry	147	104.2	83.36	20.84	0.8	0.2	3063
7	Sand	Medium dense (D_r = 40%), S_r = 50%	49	37.4	27.94	9.46	0.75	0.25	464
8	Sand	Medium dense (D_r = 40%), S_r = 50%	98	66.4	49.6	16.8	0.75	0.25	1646
9	Sand	Medium dense (D_r = 40%), S_r = 50%	147	95.4	71.26	24.14	0.75	0.25	3548
10	Sand	Dense (D_r = 80%), S_r = 50%	49	48.6	37.86	10.74	0.78	0.22	526
11	Sand	Dense (D_r = 80%), S_r = 50%	98	77.6	60.45	17.15	0.78	0.22	1681
12	Sand	Dense (D_r = 80%), S_r = 50%	147	106.6	83.04	23.56	0.78	0.22	3463
13	Sand	Medium dense (D_r = 40%), 15% fines, S_r = 50%	49	34.9	25.13	9.77	0.72	0.28	479
14	Sand	Medium dense (D_r = 40%), 15% fines, S_r = 50%	98	63.9	46.01	17.89	0.72	0.28	1753
15	Sand	Medium dense (D_r = 40%), 15% fines, S_r = 50%	147	92.9	66.89	26.01	0.72	0.28	3824
16	Sand	Dense (D_r = 70%), 15% fines, S_r = 50%	49	43.3	32.22	11.08	0.74	0.26	543
17	Sand	Dense (D_r = 70%), 15% fines, S_r = 50%	98	72.3	53.79	18.51	0.74	0.26	1814
18	Sand	Dense (D_r = 70%), 15% fines, S_r = 50%	147	101.3	75.37	25.93	0.74	0.26	3812
19	Sand	Medium dense (D_r = 45%), 25% fines, Saturated	49	33.3	22.68	10.62	0.68	0.32	521
20	Sand	Medium dense (D_r = 45%), 25% fines, Saturated	98	62.3	42.43	19.87	0.68	0.32	1948
21	Sand	Medium dense (D_r = 45%), 25% fines, Saturated	147	91.3	62.18	29.12	0.68	0.32	4281
22	Sand	Dense (D_r = 75%), 25% fines, Saturated	49	41.7	29.4	12.3	0.7	0.29	603
23	Sand	Dense (D_r = 75%), 25% fines, Saturated	98	70.7	49.84	20.86	0.7	0.3	2044
24	Sand	Dense (D_r = 75%), 25% fines, Saturated	147	99.7	70.29	29.41	0.7	0.3	4323
25	Gravel	Loose state (D_r = 35%), dry	49	42	34.78	7.22	0.83	0.17	354
26	Gravel	Loose state (D_r = 35%), dry	98	71	58.79	12.21	0.83	0.17	1197
27	Gravel	Loose state (D_r = 35%), dry	147	100	82.8	17.2	0.83	0.17	2528
28	Gravel	Dense state (D_r = 70%), dry	49	51.8	44.34	7.46	0.86	0.14	366
29	Gravel	Dense state (D_r = 70%), dry	98	80.8	69.16	11.64	0.86	0.14	1140
30	Gravel	Dense state (D_r = 70%), dry	147	109.8	93.99	15.81	0.86	0.14	2324

Table 2. *Cont.*

Sr No	Soil Group	Condition	σ_n (kPa)	S_p (kPa)	S_{ur} (kPa)	Δ (kPa)	R	I_b	E
31	Gravel	Medium dense (D_r = 45%), 5% fines, S_r = 50%	49	45.3	36.33	8.97	0.8	0.2	440
32	Gravel	Medium dense (D_r = 45%), 5% fines, S_r = 50%	98	74.3	59.59	14.71	0.8	0.2	1442
33	Gravel	Medium dense (D_r = 45%), 5% fines, S_r = 50%	147	103.3	82.85	20.45	0.8	0.2	3007
34	Gravel	Dense (D_r = 80%), 5% fines, S_r = 50%	49	55.1	45.73	9.37	0.83	0.17	459
35	Gravel	Dense (D_r = 80%), 5% fines, S_r = 50%	98	84.1	69.8	14.3	0.83	0.17	1401
36	Gravel	Dense (D_r = 80%), 5% fines, S_r = 50%	147	113.1	93.87	19.23	0.83	0.17	2826
37	Sand	Medium dense (D_r = 55%), Saturated	49	36.6	26.86	9.74	0.73	0.27	477
38	Sand	Medium dense (D_r = 55%), Saturated	98	65.6	48.15	17.45	0.73	0.27	1710
39	Sand	Medium dense (D_r = 55%), Saturated	147	94.6	69.44	25.16	0.73	0.27	3699
40	Sand	Very dense (D_r = 85%), 15% fines, Saturated	49	45.5	33.26	12.24	0.73	0.27	600
41	Sand	Very dense (D_r = 85%), 15% fines, Saturated	98	74.5	54.46	20.04	0.73	0.27	1964
42	Sand	Very dense (D_r = 85%), 15% fines, Saturated	147	103.5	75.66	27.84	0.73	0.27	4093
43	Gravel	Very dense (D_r = 85%), S_r = 50%	49	54	45.52	8.48	0.84	0.16	415
44	Gravel	Very dense (D_r = 85%), S_r = 50%	98	83	69.97	13.03	0.84	0.16	1277
45	Gravel	Very dense (D_r = 85%), S_r = 50%	147	112	94.42	17.58	0.84	0.16	2585

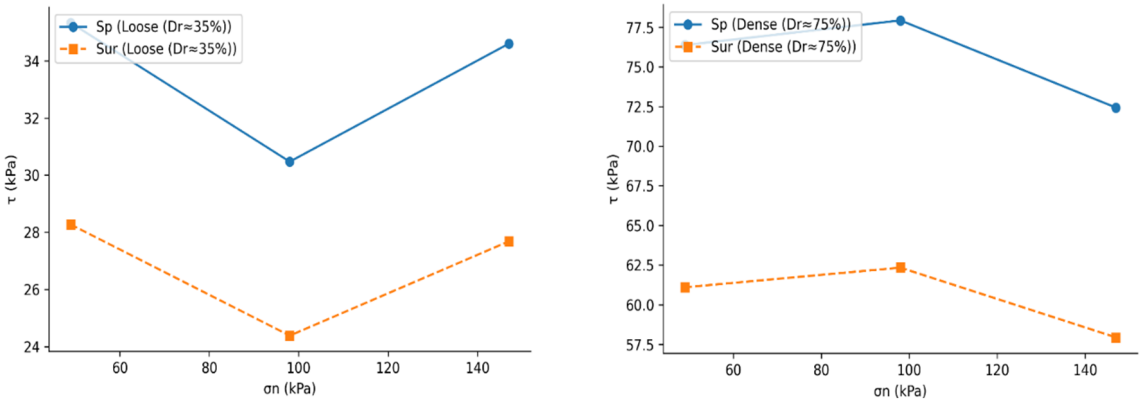

(**a**) (**b**)

Figure 8. Comparison of τ vs σ_n for loose (**a**)-D_r of 35% and dense (**b**) D_r of 75% sand for S_p & S_{ur}.

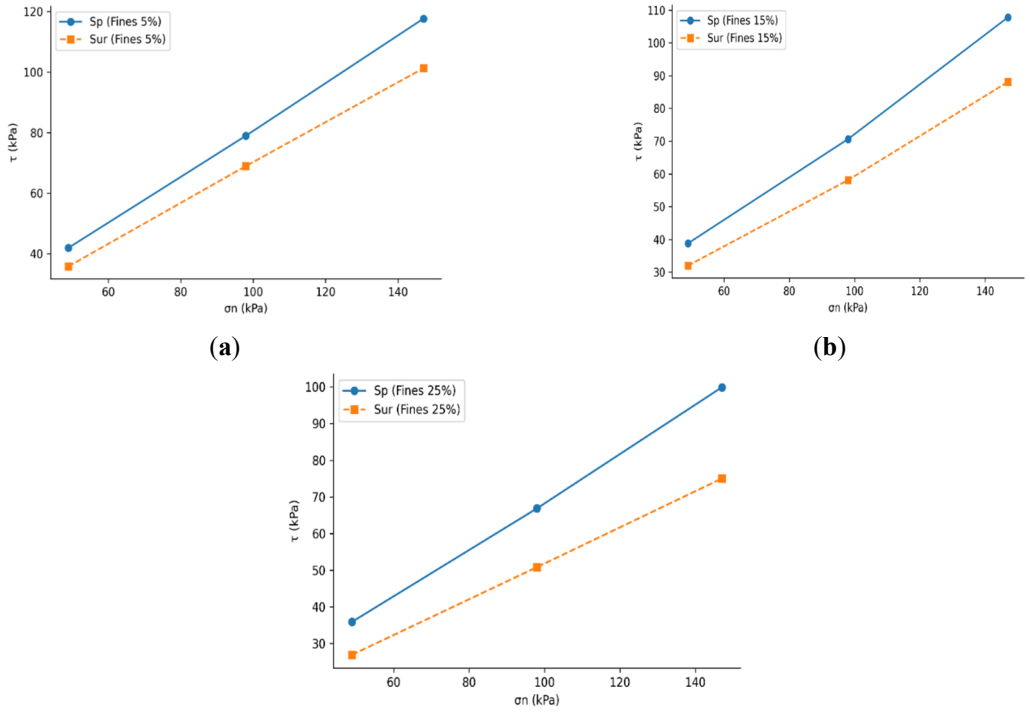

(**a**) (**b**)

(**c**)

Figure 9. Comparison of τ versus σn for sand with varying percentages of fines: (**a**) 5% fines content (gravel) , (**b**) 15% fines content (sand), and (**c**) 25% fines content (sand) for S_p & S_{ur}.

4.3.2. Effect of Fines Content (5%, 15%, 25%)

From the τ–σ_n plots in Figure 9, it is evident that fines content has a dual influence on shear strength. At lower fines levels (around 5 to 15%), both S_p and S_{ur} increase steadily with normal stress, which suggests that a small number of fines helps densify the grain skeleton by filling voids and improving particle interlock. However, once fines content reaches 25%, the trend starts to reverse as S_p and S_{ur} begin to drop, indicating that excessive fines no longer reinforce the structure but instead behave like a lubricant layer, reducing friction between sand grains.

This shift is also reflected in the strength loss parameter Δ, which increases consistently with fines content, especially at higher σ_n. That means more fines lead to higher brittleness, even when the absolute strength starts to fall. In other words, fines initially make the material stronger but also make it more sensitive to post-peak collapse, and beyond a certain limit, fines weaken the entire structure while still amplifying the strength drop.

4.3.3. Effect of Saturation (S_r = 0% to 100%)

The influence of saturation on shear strength behaviour is clearly visible across Figure 10a–d. In the dry condition (Figure 10a), the sand mobilises the highest S_p due to strong dilatancy and suction effects, but this also results in the largest post-peak strength loss, indicating a distinctly brittle failure response. As the degree of saturation increases to 50% and 70% (Figure 10b,c, with the S_r = 70% series obtained from supplementary laboratory tests excluded from the 45-case primary modeling dataset in Table 2), both peak and residual strengths continue to rise with normal stress, but the gap between them becomes slightly smaller compared to the dry state, suggesting that partial saturation still promotes dilative resistance but with slightly moderated brittleness. A major shift occurs at full saturation (Figure 10d), where peak and residual curves move much closer together, particularly at higher normal stresses. This reduced separation signifies that pore-water pressure suppresses dilatancy and strain localisation, leading to a more ductile sliding mechanism with lower Δ and higher R values. Overall, increasing saturation transitions the material response from strong but brittle (dry and partially saturated) to weaker but more stable (fully saturated), which is critical when assessing failure mode under drained or undrained field conditions.

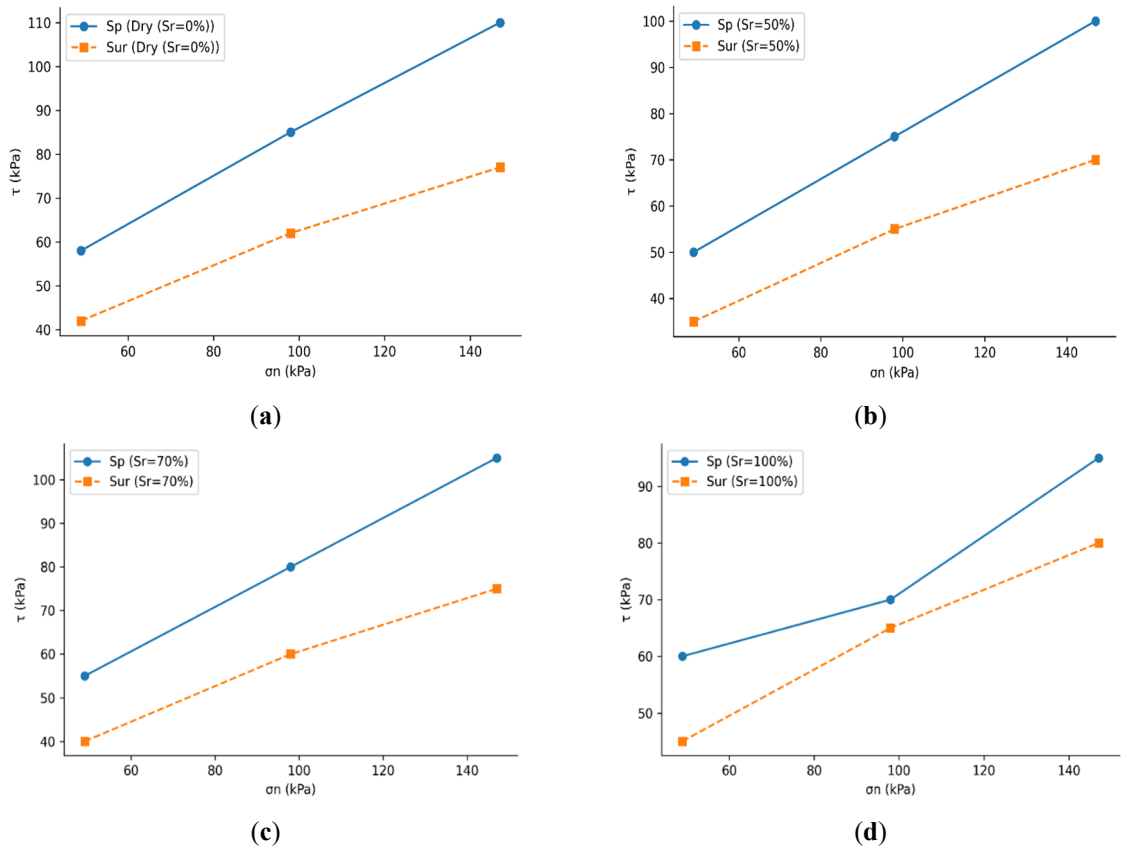

Figure 10. Comparison of τ versus σ_n for sand under varying degrees of saturation (S_r): (**a**) S_r = 0% (dry condition), (**b**) S_r = 50%, (**c**) S_r = 70%, and (**d**) S_r = 100% (fully saturated condition).

4.4. Strength Degradation and Residual Strength Mobilization Parameters

The three figures below (Figures 11–13) show variations of the strength reduction from S_p to S_{ur} under different D_r, fines ratio, S_r, and σ_n. Figure 11 depicts variations of the four descriptors of strength-degradation (Δ, R, I_b, and E), whereas Figure 12 shows the heat maps depicting the numerical values of the four descriptors to enable comparison of the values under different conditions. The variations of the four strength reduction descriptors have been presented in Figure 13 in the form of radar plots at 49, 98, and 147 kPa of normal stress. Both the heat maps and radar plots provide additional descriptions of the variations; nevertheless, none of them provides statistically significant results on their own.

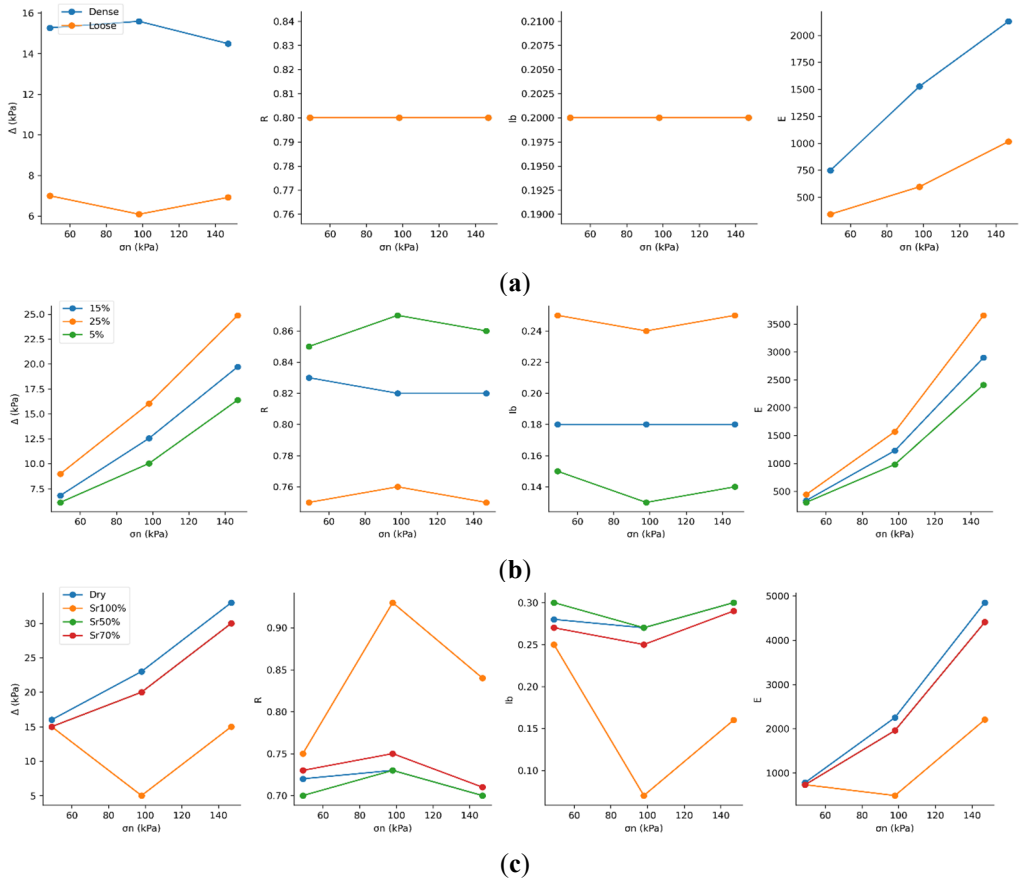

Figure 11. Comparative analysis of strength degradation parameters (Δ, R, I_b, E) with σ_n across (**a**) relative density (**b**) fines% (**c**) saturation.

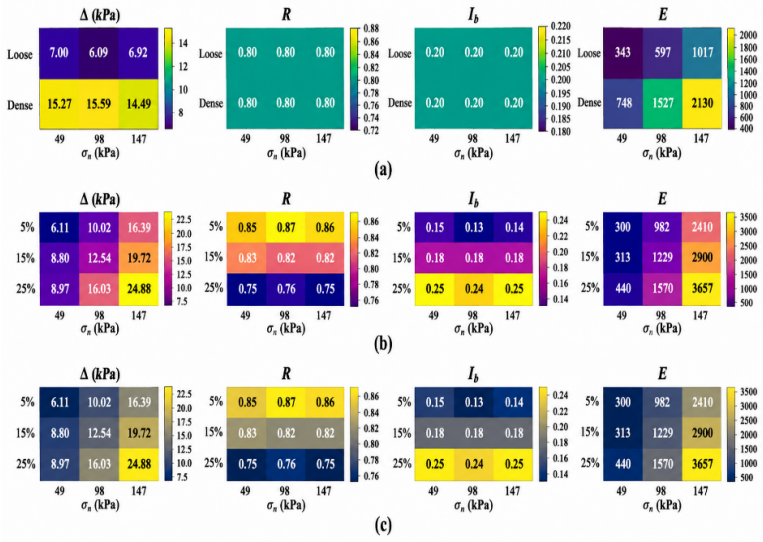

Figure 12. Comparative heatmap matrix of shear strength degradation metrics (Δ, R, I_b, E) across laboratory conditioning factors: (**a**) relative density (**b**) fines% (**c**) saturation.



Figure 13. Radar-based comparative analysis for (**a**) Δ (**b**) R (**c**) I_b and (**d**) E across conditioning variables (D_r, fine% and S_r).

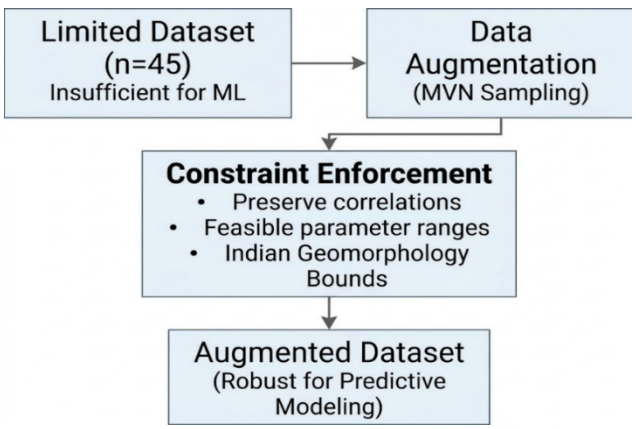

Figure 14. Structured data augmentation framework illustrating MVN-based sampling with geotechnical constraint enforcement to generate a physically consistent augmented dataset for predictive modeling.

5. Synthetic Data Augmentation and Multivariate Regression

5.1. Data Expansion: Multivariate Normal Distribution (MVN)

The model development is integrally limited to 45 DST/RDST samples each for sand and gravel, that is insufficient for development of large-scale geotechnical modeling, majorly when considering the framework to India-scale applications. Here comes the necessity of a systematic data expansion approach that not only increases the dataset size but also preserves the physical properties of soil behavior. To account this challenge here used a probabilistic data augmentation approach based on the MVN was utilized. This augmentation was meant to increase the size of the data set without changing the statistical properties or geotechnical conditions found in the physical observations available. These augmented data samples have been used in the models and cannot be regarded as independent experimental trials. Therefore, the predictive performance presented needs to be understood relative to the physical data sample size and validation approach used.

A comparative assessment of MVN augmentation and alternative data augmentation techniques, highlighting their limitations and the advantages of the proposed MVN approach in preserving the covariance structure and geotechnical consistency, is presented in Table 3. Mathematically, the augmented dataset is generated by sampling from a MVN distribution defined as:

$$X \sim N(\boldsymbol{\mu}, \boldsymbol{\Sigma}) \tag{11}$$

where $\boldsymbol{\mu}$ preserves central tendency, $\boldsymbol{\Sigma}$ maintains data spread, and covariance retains critical inter-parameter relationships for geotechnical consistency.

Table 3. Comparative analysis between MVN & alternative augmentation methods.

Method	Problem	Why MVN Wins
Random Sampling	Breaks parameter relationships	Unrealistic soil behaviour
Bootstrapping	No new physics introduced	Limited diversity
GAN/VAE	Black-box approach	No geotechnical control
SMOTE	Linear interpolation only	Destroys soil mechanics
MVN (Proposed)	Preserves covariance structure	Physics + statistics aligned

5.2. Physics Constrained MVN Augmentation and Calibration

In above section the statistical covariance alone does not guarantee physically admissible soil states, the generated observations were subsequently screened using the constraints given in Table 4.

Table 4. Physics constraints for MVN generation.

Constraint	Rule	Physical Basis
Relative Density Bounds	$20\% \le D_r \le 95\%$	IS:1498
Strength Limit	$0 < S_{ur} < S_p$	Mohr column failure criterion
Void Ratio Consistency	$e = e_{max} - D_r (e_{max} - e_{min})$	Phase relationship
Degree of Saturation	$0 \le S_r \le 100\%$	Physical saturation limit
Fines Content	Soil group specific limits	Consistency with representative soil classes
DCPT Resistance	$N_d > 0$	Physical penetration-resistance requirement

For integration with datasets lacking direct DCPT measurements, N_d was subsequently estimated from measurable soil state parameters. Relative density exhibited the strongest association with N_d ($r = 0.983$), followed by void ratio ($r = -0.627$), whereas the direct association with normal stress was comparatively weak ($r = 0.141$). Accordingly, a simplified density based relationship and a multivariate physics informed relationship were evaluated:

$$N_d = 0.578 D_r - 5.35 \tag{12}$$

and

$$N_d = 0.614 D_r + 0.010 \sigma_n + 8.27 e - 12.39 \tag{13}$$

where N_d is the DCPT blow count (blows/30 cm), D_r is relative density (%), σ_n is normal stress (kPa), and e is void ratio. The developed equations predict S_{ur} within the range of the experimental conditions investigated; their applicability to post-liquefaction conditions remains unverified. Since N_d is estimated from soil-state parameters and D_r is interrelated with e, the resulting relationships are interpreted as empirical predictive correlations, and their performance is limited to the adopted dataset and estimation procedure.

6. Laboratory Based Equation Development

The empirical S_{ur} relationships were developed using controlled DST/RDST observations obtained from 45 samples of coarse grain soil of sand and gravel each. The RDST measurements were used to characterize the post-peak response and determine the S_{ur} under progressive shearing. The regression framework was formulated using parameters having direct geotechnical relevance, namely σ_n, D_r, e, and N_d. For the gravelly dominated soils, median particle size d_{50} was additionally included as a predictor to account for the potential influence of particle size on interlocking and dilatancy. The observed values refer to the physical tests conducted and contained within the experimental data set. Since deviation in results was not separately reported, neither was uncertainty in measurements, the extent of repeatability of the experiment cannot be evaluated from the data provided. Therefore, the strength observed values and regression statistics should be considered in light of the data set only.

The suitability of the selected predictors was initially examined using the correlation matrices presented in Figure 15. For sand, S_{ur}^{lab} exhibited strong positive correlations with σ_n ($r = 0.90$), N_d ($r = 0.83$), and D_r ($r = 0.79$), while e showed a negative correlation ($r = -0.69$). The correlation with S_r was weak ($r = 0.08$). A similar pattern was observed for gravel, with S_{ur}^{lab} correlated with σ_n ($r = 0.88$), N_d ($r = 0.86$), and D_r ($r = 0.83$), while e showed a negative correlation ($r = -0.73$) and S_r exhibited only a weak relationship ($r = 0.05$). These results support the selection of σ_n, D_r, e, and N_d as the principal predictors in the MLR formulation.

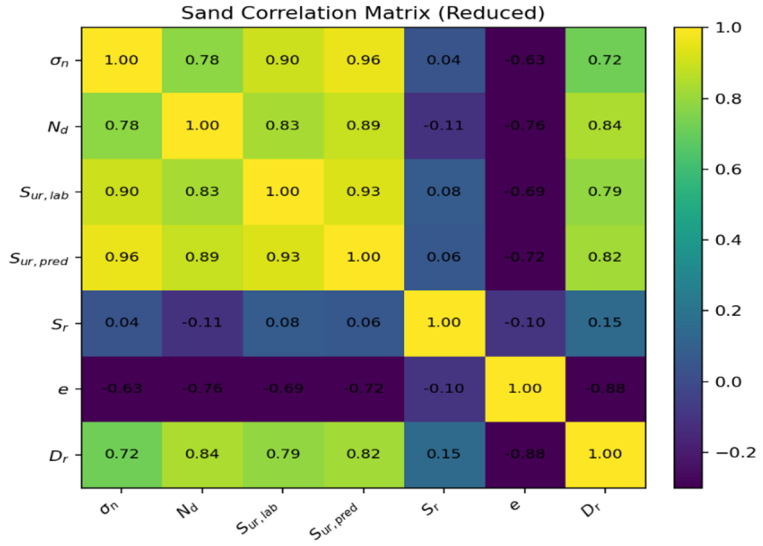

(**a**)

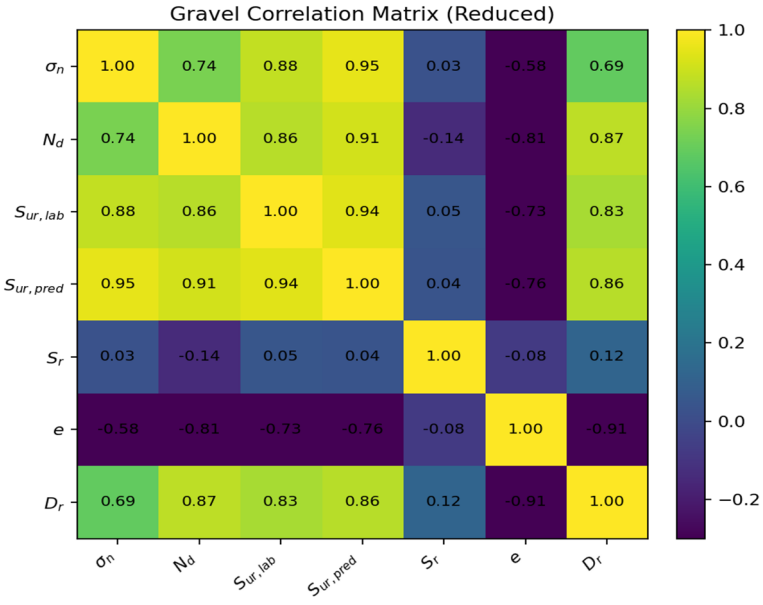

(**b**)

Figure 15. Correlation matrices showing the relationships among σ_n, D_r, e, S_r, N_d, and S_{ur} for (**a**) sand and (**b**) gravel.

The MLR formulation was used to quantify the combined contribution of the selected variables while maintaining an explicit and physically interpretable relationship suitable for engineering application. The regression coefficients were estimated by minimizing the differences between the measured and predicted S_{ur} values. Based on the material-specific behaviour, separate empirical relationships were obtained for sand- and gravel-dominated soils.

For sand-dominated soils classified as SP, SW, SM, and SC, the fitted MLR relationship was obtained as

$$S_{ur} = 0.58 \cdot \sigma_n + 0.40 \cdot D_r + 0.15 \cdot N_d - 0.99 \cdot e - 22.8 \quad (14)$$

For gravel-dominated soils classified as GP and GW, the corresponding relationship was

$$S_{ur} = 1.15 \cdot \sigma_n + 0.75 \cdot D_r + 0.15 \cdot N_d - 0.99 \cdot e - 0.50 d_{50} - 25 \quad (15)$$

where d_{50} is the median particle diameter (in mm) obtained from sieve analysis, spanning $d_{50} = 4.75 - 12.5$ mm across the GP and GW gravel dataset (specifically $d_{50} = 8.5$ mm for clean gravel and $d_{50} = 7.8$ mm for 5% fines gravel in Table 2). The inclusion of d_{50} in the gravel model improved prediction accuracy by approximately 6%, indicating the potential contribution of particle-size-dependent interlocking and dilatancy to the shear-strength response of coarse materials. To outspread the applicability to field conditions with rounded particles, an angularity correction is introduced:

$$S_{ur,\,rounded} = 0.85 \times S_{ur,\,predicted} \quad (16)$$

7. Validation of the Developed MLR Framework for S_{ur} Prediction

Following MVN augmentation, the expanded database was subjected to covariance, physical, statistical, predictive, and reliability checks to assess the robustness of the developed MLR framework. Cholesky decomposition was used to preserve the multivariate covariance structure, while the geotechnical constraints described in Table 4 were applied to reject physically inadmissible observations. For the retained dataset, the mean correlation difference between experimental and synthetic data decreased from 0.379 to 0.111, representing a 70.8% improvement, with correlation recovery of 89.2% for $\sigma_n - D_r$ and 85.8% for $\sigma_n - N_d$. The calibrated N_d relationships were subsequently used for datasets lacking direct DCPT measurements. The multivariate formulation provided $R^2 = 0.972$, with an independent validation MAE of approximately 2.5 blows (4.8%). Statistical comparability between experimental and synthetic observations was examined using Tukey's HSD at $\alpha = 0.05$, with the associated effect-size analysis indicating small differences in S_{ur} ($d < 0.4$).

Predictive verification was performed separately for sand and gravel (Figure 16). The sand dataset yielded $R^2 = 0.941$, RMSE = 4.08 kPa, MAE = 3.27 kPa and bias = −0.09 kPa, whereas the gravel dataset yielded $R^2 = 0.932$, RMSE = 4.65 kPa, MAE = 3.87 kPa and bias = 1.05 kPa. The near-unity regression slopes (0.983 and 1.020) and close agreement with the 1:1 line indicate limited systematic prediction error. Nevertheless, these values of R^2 measure the goodness-of-fit for the dataset analysed, but do not, on their own, provide evidence of independent predictive ability.

However, these values of R^2 refer to the extent of variation accounted for by the regression equations in the dataset used for the evaluation and need to be considered together with the RMSE, MAE, bias, and slopes of regression. Even though the obtained indices, along with close to unity regression slopes, provide evidence of satisfactory correspondence between the predicted and measured residual shear strength, these indices do not ensure by themselves the ability of the model to predict the behaviour of independent datasets and the application of the developed relationship to other types of soils.

Finally, 10,000 Monte Carlo simulations were performed to quantify uncertainty in the predicted S_{ur}. The resulting distribution had a mean of approximately 239 kPa, standard deviation of 81 kPa, and COV of 0.23–0.34, with an estimated reliability index of $\beta = 1.64$ under the adopted limit-state definition. The reliability result is therefore conditional on the specified limit state and is used as an uncertainty assessment rather than as a universal failure probability.

As a whole, the findings illustrate that the augmented database has preserved the main statistical correlations from the experimental data, taking into account the constraints set for the geotechnical data. The created MLR model has been validated and assessed in terms of reliability to estimate its predictability and uncertainties. The obtained MVN-MLR framework allows using the empirical formulas to predict S_{ur} for the Indian soils. However, for other regions, an independent validation is needed.

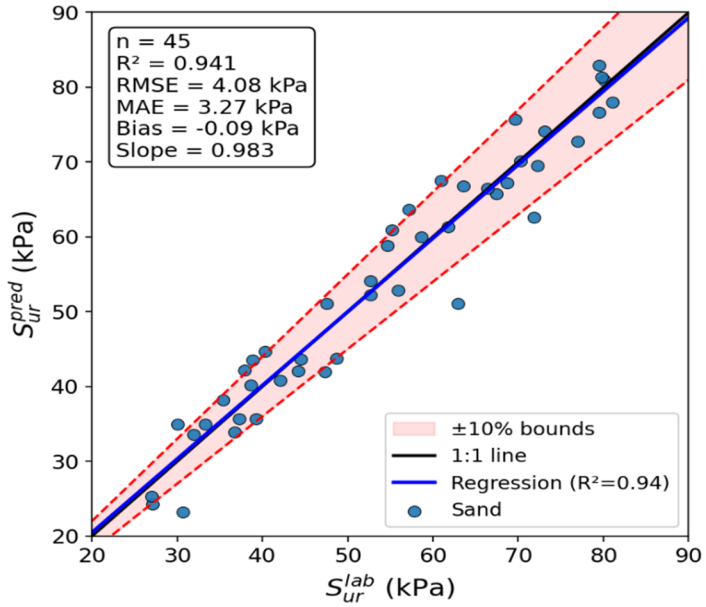

(**a**)

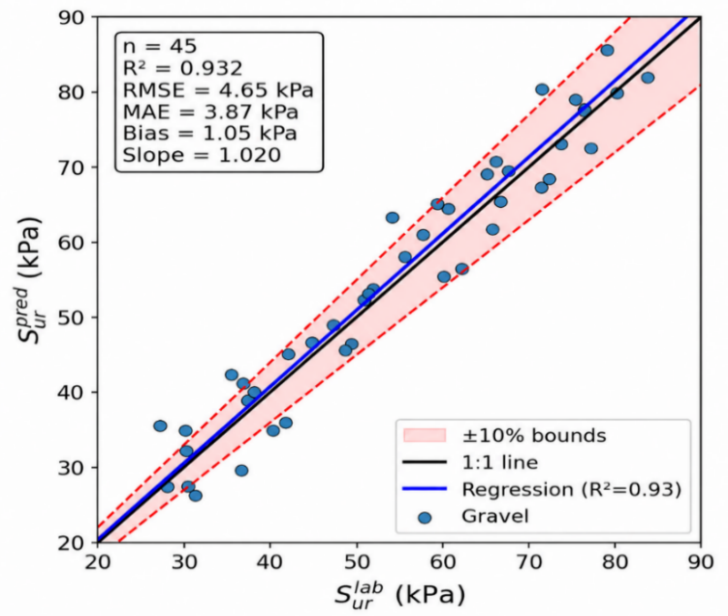

(**b**)

Figure 16. Comparison of predicted and measured S_{ur} for (**a**) sand and (**b**) gravel.

8. Regional S_{ur} Zonation of Coarse-Grained Soils across India

To demonstrate the regional applicability of the developed DCPT–S_{ur} framework, the empirical equations developed for sand- and gravel-dominated soils were applied to representative geotechnical conditions across major Indian states and Union Territories. For each region, representative values of soil classification, relative density, void ratio, degree of saturation, normal stress, and DCPT resistance were assigned based on the dominant depositional environment and typical coarse-grained soil characteristics reported for the region. These representative parameters were then used as inputs to the corresponding material-specific S_{ur} equation.

The resulting representative S_{ur} values were spatially interpolated/classified at the state level to produce the zonation map shown in Figure 17. The map therefore represents a model-based regional estimate of residual shear strength, rather than direct measurements at every location, and is intended primarily to demonstrate the potential application of the developed DCPT–S_{ur} relationship at a regional scale.

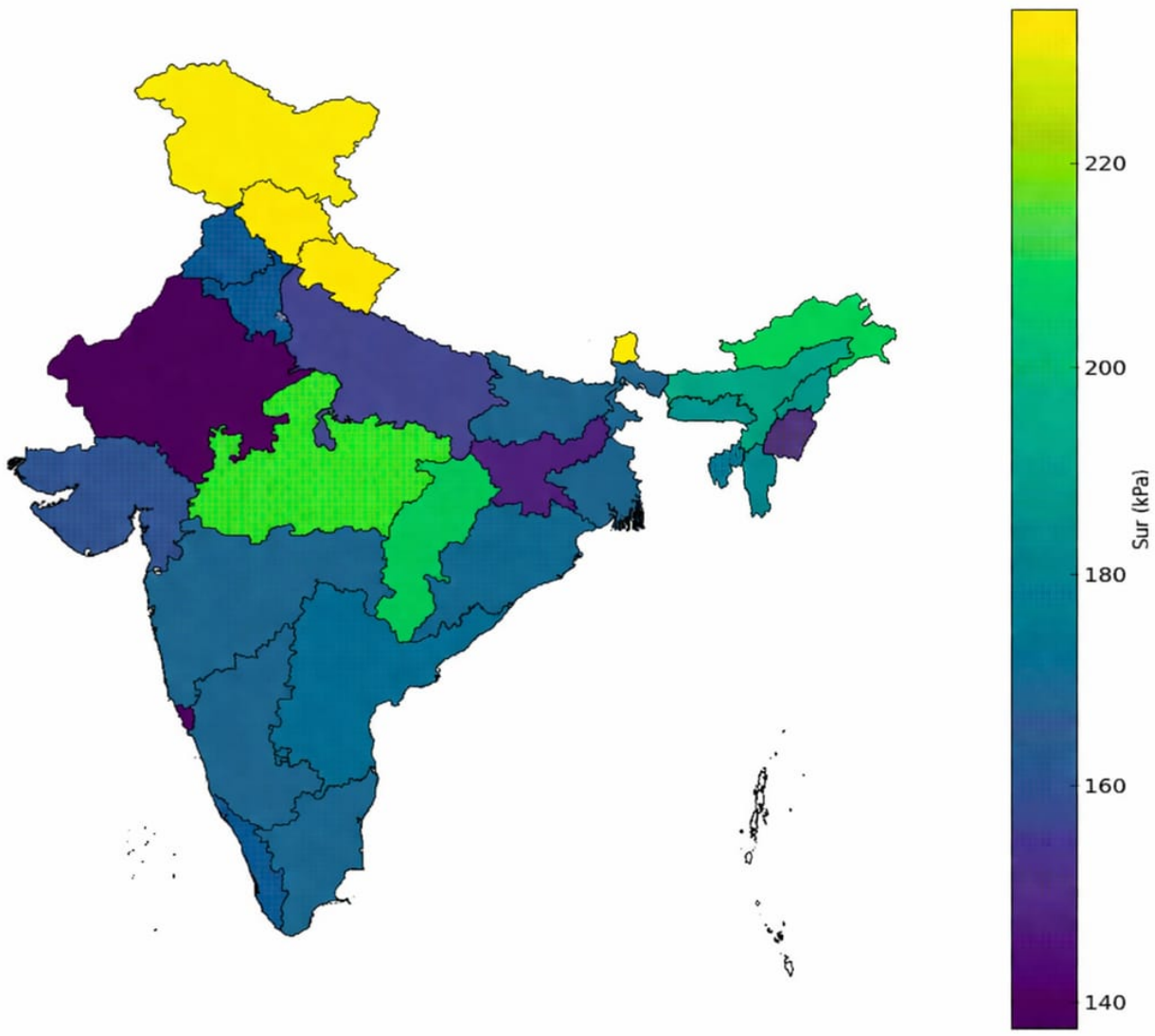

Figure 17. State-wise zonation map of S_{ur} for coarse-grained soils across India, obtained by applying the DCPT–S_{ur} empirical equation to representative regional soil and DCPT conditions.

The spatial pattern indicates comparatively higher representative S_{ur} values in regions where dense sands and gravelly deposits are prevalent, including parts of Rajasthan, Gujarat, Jammu and Kashmir, Himachal Pradesh, and Uttarakhand. The higher values are associated primarily with greater relative density, lower void ratio, and the greater mechanical interlocking characteristic of dense granular deposits. In contrast, regions dominated by silty or clayey sands and saturated alluvial or deltaic deposits, particularly parts of Bihar, West Bengal, Odisha, Assam, and eastern Uttar Pradesh, generally exhibit lower representative S_{ur} values because of increased fines content, higher moisture conditions, and less favourable packing.

Intermediate S_{ur} values occur across several peninsular and coastal regions, including Maharashtra, Karnataka, Telangana, Andhra Pradesh, and Tamil Nadu, where residual, lateritic, coastal, and mixed alluvial deposits produce greater spatial variability in density, fines content, and saturation. The resulting zonation therefore reflects the combined influence of soil type, density, stress state, particle characteristics, and moisture condition rather than geographical location alone.

The classifications represent dominant or representative coarse-grained deposits and should not be interpreted as implying uniform soil conditions throughout an entire state. The soil-type classification in Table 5 provides the geological basis for interpreting the spatial pattern shown in Figure 17. To further quantify the expected differences among the principal IS: 1498 soil groups, representative S_{ur} values and ranges are summarized in Table 6.

The results in Table 6 indicate a general trend of higher residual strength for gravelly soils than for sandy soils, with GP showing the highest representative value, followed by GW, SW, SP, SM, and SC. This trend is consistent with the increasing influence of particle interlocking, density, and packing characteristics on the residual resistance of coarse-grained materials. The lower values associated with SM and SC reflect the potential influence of fines on particle interaction and the greater sensitivity of these materials to saturation and moisture conditions.

Table 5. Dominant coarse-grained soil types across India (IS: 1498).

State/UT	Coarse-Grained Soil	Typical Deposits	Remarks for S_{ur}
Rajasthan	SP, SW, GP	Aeolian dunes, desert sands	High S_{ur} due to density
Haryana	SW, SP–SM	Fluvio-aeolian	Very good post-liquefaction stability
Punjab	SW, SP–SM	Indo-Gangetic alluvium	High S_{ur} good post-liquefaction stability
Gujarat	GW, GP, SP	Coastal & alluvial	High stiffness, high S_{ur}
Madhya Pradesh	GP, GW, SP	Alluvial–residual	Medium–high S_{ur}
Uttar Pradesh	SM, SP-SC	Ganga alluvium	Lower S_{ur} in eastern belt
Bihar	SM–SC	Alluvial plains	Fines reduce S_{ur}
West Bengal	SM–SC	Deltaic alluvium	Low S_{ur}, high S_r
Assam	SM–SC	Brahmaputra alluvium	Saturation controls S_{ur}
Maharashtra	SW–SM	Lateritic + coastal	Moderate S_{ur}
Karnataka	SC–SM	Lateritic soils	Moderate S_{ur}, moisture sensitive
Tamil Nadu	SP–SM	Coastal sands	Variable S_{ur}
Telangana	SM	Residual weathered	Medium S_{ur}
Andhra Pradesh	SM–SP	Coastal belts	Moderate S_{ur}
Odisha	SM–SC	Coastal alluvium	Fine content reduces S_{ur}
Kerala	SM–SC	Marine sands	Moisture-sensitive
J&K	GW–GP	Valley deposits	High S_{ur} (dense gravelly sands)
Himachal	GP–GW	Hill–valley	High S_{ur}
Uttarakhand	GW–GP	Terraced/alluvial fans	Dense, high S_{ur}
NE States	SM–SC	High rainfall systems	Saturation reduces S_{ur}

Table 6. Soil type vs S_{ur} range summary.

Soil Type (IS: 1498)	Mean S_{ur} (kPa)	Typical Range	Region Examples
GP Poorly graded gravel	210	180–260	Gujarat, MP, J&K
GW—Well graded gravel	195	160–240	Uttarakhand, Himachal
SP—Poorly graded sand	170	140–210	Rajasthan, Haryana
SW—Well-graded sand	185	155–230	Gujarat, Punjab
SM—Silty sand	165	140–200	Telangana, AP
SC—Clayey sand	150	110–180	Bihar, WB, Odisha

Overall, the spatial analysis demonstrates how the developed DCPT–S_{ur} equations can be extended from controlled laboratory observations to a regional engineering framework. The map and accompanying tables provide a first-order representation of the expected spatial variability of S_{ur} in coarse-grained soils across India. However, the zonation should be interpreted as a screening- and planning-level model, and site-specific investigation remains necessary for detailed design because local variations in density, fines content, groundwater conditions, particle characteristics, and stress history may produce substantial deviations from the representative state-wise values.

9. Discussion

The results demonstrate that the proposed degradation parameters Δ, R, I_b, and E provide complementary measures of post-peak behaviour in coarse-grained soils. The observed variations in these descriptors reflect changes in density, packing, fines content, saturation, and stress level, allowing the transition from peak to residual strength to be interpreted using physically meaningful parameters. Their combined use provides a more informative description of strain-softening behaviour than residual strength alone. The developed relationships further establish a direct link between laboratory residual strength and field-measurable penetration resistance. Separate formulations for sand- and gravel-dominated soils account for their differing particle-scale behaviour, while the inclusion of d_{50} in the gravel formulation captures the additional influence of particle size and interlocking. The resulting relationships provide a practical means of estimating S_{ur} where direct residual-strength testing is limited.

The predictive results support this interpretation, with $R^2 = 0.941$ for sand and $R^2 = 0.932$ for gravel in the reported prediction assessment. The close agreement between measured and predicted values, together with low bias and near-unity regression slopes, indicates that the proposed framework captures the dominant trends governing residual strength within the investigated parameter range.

10. Limitations and Scope of Applicability

The results should be interpreted within the range of the experimental and augmented datasets. Particle angularity was not explicitly parameterised, although it can influence interlocking, dilatancy, and post-peak response. Gradation descriptors such as C_u and C_c were also not explicitly incorporated and may become important for well-

graded or gap-graded materials. The pore-pressure response was represented through the adopted saturation and direct-shear framework and therefore does not fully reproduce transient cyclic or undrained conditions.

Although the MVN augmentation was constrained using observed covariance relationships and geotechnical limits, synthetic observations remain model-dependent and should not be considered equivalent to additional physical experiments. Accordingly, extrapolation beyond the investigated ranges of D_r, N_d, stress, particle characteristics, and saturation should be undertaken cautiously. The proposed relationships are therefore most appropriate for screening, preliminary assessment, and regional-scale estimation, while site-specific testing remains necessary for high-consequence design.

11. Integrated Interpretation and Engineering Implications

The principal contribution of the study is the integration of experimental S_{ur} measurements, physics-constrained statistical augmentation, field penetration resistance, and interpretable regression modelling into a single framework. MVN augmentation extends the available parameter space while Cholesky decomposition preserves the observed multivariate structure; geotechnical constraints control physical admissibility; and N_d calibration enables application to datasets without direct DCPT measurements. The resulting framework provides a practical connection between laboratory post-peak behaviour and field-scale characterization. The India-wide zonation demonstrates how the equations can be translated into a regional engineering tool using representative soil and DCPT conditions.

The proposed approach therefore provides two complementary outputs: (i) strength-degradation indicators and (ii) an empirical framework for estimating S_{ur} from accessible geotechnical parameters. This combination enhances the potential application of the work to preliminary seismic assessment, post-liquefaction stability screening, embankment and slope evaluation, and regional geotechnical planning.

12. Conclusions

This study developed an integrated framework for characterizing and predicting S_{ur} of coarse-grained soils. The principal conclusions are:

Four interpretable strength-degradation indicators Δ, R, I_b, and E provided complementary measures of post-peak strength degradation and energy dissipation, enabling a more comprehensive interpretation of strain-softening behaviour.

Physics-constrained MVN augmentation, supported by Cholesky covariance preservation, retained the principal multivariate relationships of the experimental database while expanding the parameter space for regression modelling.

DCPT calibration provided a practical bridge between laboratory and field characterization, with the multivariate N_d relationship achieving $R^2 = 0.972$ and an independent MAE of approximately 2.5 blows (4.8%).

Material-specific MLR equations were developed for sand- and gravel-dominated soils, with the gravel formulation incorporating d_{50} to account for particle-size effects. The developed relationships showed strong agreement between measured and predicted S_{ur}.

Integrated validation demonstrated consistent predictive performance, with reported R^2 values of 0.941 for sand and 0.932 for gravel, accompanied by low prediction errors and near-unity regression slopes.

Monte Carlo analysis using 10,000 simulations provided an additional assessment of prediction uncertainty, yielding a stable S_{ur} distribution and a reliability index of $\beta = 1.64$ under the adopted limit-state definition.

Regional application of the developed equations produced a state-wise S_{ur} zonation for coarse-grained soils across India, demonstrating the potential of the framework for preliminary regional assessment while recognizing the need for site-specific investigation for detailed design.

Overall, the study establishes a physics-informed, statistically controlled, and field-oriented framework linking post-peak soil mechanics with DCPT-based residual-strength estimation. The combination of mechanistic degradation descriptors, validated empirical prediction, and regional zonation provides a practical basis for extending residual-strength assessment from controlled laboratory conditions to engineering-scale applications.

Author Contributions

S.V.S.: Conceptualization, methodology, investigation, experimental setup, data curation, formal analysis, visualization, software, validation, writing—original draft preparation, and writing—review and editing. S.G.: Conceptualization, methodology, supervision, and writing—review and editing. F.H.: Data analysis, formal analysis, and writing—review and editing. All authors have read and agreed to the published version of the manuscript.

Funding

This research received no external funding. The experimental investigations were carried out in the laboratory facilities of the Department of Civil Engineering, Sharda University, Greater Noida, Uttar Pradesh, India, as part of the doctoral research of Shubhendu Vikram Singh. No external grant or sponsored research funding was received for this work.

Institutional Review Board Statement

Not applicable.

Informed Consent Statement

Not applicable.

Data Availability Statement

The experimental data generated during this study, including the Direct Shear Test (DST) and Reverse Direct Shear Test (R-DST) results, are available from the corresponding author upon reasonable request. The augmented dataset generated using the Multivariate Normal Distribution (MVN) approach is derived from the original experimental observations and is also available upon reasonable request. The authors are committed to providing access to the relevant data to support verification and reproducibility of the research findings.

Acknowledgments

The authors gratefully acknowledge the Department of Civil Engineering, Sharda University, Greater Noida, Uttar Pradesh, India, for providing laboratory facilities and institutional support for conducting the experimental investigations. The authors also acknowledge the technical assistance and support received during the laboratory testing activities.

Conflicts of Interest

The authors declare no conflict of interest.

Use of AI and AI-Assisted Technologies

No AI tools were utilized for this paper.

References

1. ABG Ltd. *Soil Properties: Shear Strength*; Technical Note. ABG Ltd.: Meltham, UK, 2021.
2. Ishihara, K. Liquefaction and flow failure during earthquakes. *Géotechnique* **1993**, *43*, 351–451. https://doi.org/10.1680/geot.1993.43.3.351.
3. Norris, G.; Siddharthan, R.; Zafir, Z.; et al. Liquefaction and residual strength of sands from drained triaxial tests. *J. Geotech. Geoenviron. Eng.* **1997**, *123*, 220–228. https://doi.org/10.1061/(ASCE)1090-0241(1997)123:3(220).
4. Castro, G.; Seed, R.B.; Keller, T.O.; et al. Steady-State Strength Analysis of Lower San Fernando Dam Slide. *J. Geotech. Eng.* **1992**, *118*, 406–427. https://doi.org/10.1061/(asce)0733-9410(1992)118:3(406).
5. Dewoolkar, M.; Hargy, J.; Anderson, I.; et al. Residual and post-liquefaction strength of a liquefiable sand. *J. Geotech. Geoenviron. Eng.* **2016**, *142*, 04015068. https://doi.org/10.1061/(ASCE)GT.1943-5606.0001374.
6. Olson, S.M.; Stark, T.D. Liquefied strength ratio from liquefaction flow failure case histories. *Can. Geotech. J.* **2002**, *39*, 629–647. https://doi.org/10.1139/t02-001.
7. Idriss, I.M.; Boulanger, R.W. 2nd Ishihara Lecture: SPT- and CPT-based relationships for the residual shear strength of liquefied soils. *Soil Dyn. Earthq. Eng.* **2015**, *68*, 57–68. https://doi.org/10.1016/j.soildyn.2014.09.010.
8. Moss, R.E.S. Liquefied Strength and Its Relationship to Effective Stress. *J. Geotech. Geoenviron. Eng.* **2020**, *146*, 06020024. https://doi.org/10.1061/(asce)gt.1943-5606.0002391.
9. Byrne, P.M.; Imrie, A.S.; Morgenstern, N.R. Results and implications of seismic performance studies for Duncan Dam. *Can. Geotech. J.* **1994**, *31*, 979–988. https://doi.org/10.1139/t94-112.
10. Yang, Y.; Kavazanjian, E. Newmark Analysis of Lateral Spreading Induced by Liquefaction. *J. Earthq. Eng.* **2022**, *26*, 3034–3053. https://doi.org/10.1080/13632469.2020.1784316.
11. Yang, Y.; Lin, Z.; Lu, H.; et al. Prediction of liquefaction-induced lateral spreading based on Neural network. *J. Vibroeng.* **2024**, 26, 657–672. https://doi.org/10.21595/jve.2023.23656.

12. Gebhart, T.R. Post-Liquefaction Residual Strength Assessment of the Las Palmas, Chile Tailings Failure. Master's Thesis, California Polytechnic State University, San Luis Obispo, CA, USA, 2016. https://doi.org/10.15368/theses.2016.130.
13. Olson, S.M. Liquefaction Analysis of Level and Sloping Ground Using Field Case Histories and Penetration Resistance. Ph.D. Thesis, University of Illinois at Urbana-Champaign, Champaign, IL, USA, 2001.
14. Ghorbani, E.; Rajabi, A.M. A review on SPT-based liquefaction potential evaluation to assess the possibility of performing a risk management. *Sci. Iran. Trans. A Civ. Eng.* **2020**, *27*, 639–656. https://doi.org/10.24200/sci.2018.5664.1413.
15. Boulanger, R.W.; Idriss, I.M. *CPT and SPT Based Liquefaction Triggering Procedures*; Report No. UCD/CGM-14/01; University of California: Davis, CA, USA, 2014.
16. Robertson, P.K. Evaluation of Flow Liquefaction and Liquefied Strength Using the Cone Penetration Test. *J. Geotech. Geoenviron. Eng.* **2010**, *136*, 842–853. https://doi.org/10.1061/(ASCE)GT.1943-5606.0000286.
17. Singh, S.V.; Ghani, S. Applications of Dynamic Cone Penetration Test for Estimating Liquefaction Susceptibility Using Machine Learning Paradigms. *Transp. Infrastruct. Geotechnol.* **2025**, *12*, 65. https://doi.org/10.1007/s40515-024-00520-5.
18. Singh, S.V.; Ghani, S. A smarter approach to liquefaction risk: Harnessing dynamic cone penetration test data and machine learning for safer infrastructure. *Front. Built Environ.* **2024**, *10*, 1495472. https://doi.org/10.3389/fbuil.2024.1495472.
19. Özener, P. Estimation of residual shear strength ratios of liquefied soil deposits from shear wave velocity. *Earthq. Eng. Eng. Vib.* **2012**, *11*, 461–484. https://doi.org/10.1007/s11803-012-0134-0.
20. Kumar, S.S.; Dey, A.; Krishna, A.M. Liquefaction Potential Assessment of Brahmaputra Sand Based on Regular and Irregular Excitations Using Stress-Controlled Cyclic Triaxial Test. *KSCE J. Civ. Eng.* **2020**, *24*, 1070–1082. https://doi.org/10.1007/s12205-020-0216-x.
21. Anderson, I.; Hargy, J.; de Alba, P.; et al. Measurement of Residual Strength of Liquefied Soil in Centrifuge Models. In Proceedings of the GeoCongress 2012, Oakland, CA, USA, 25–29 March 2012; pp. 1740–1749. https://doi.org/10.1061/9780784412121.179.
22. British Standards Institution (BSI). *BS 1377-7:1990: Methods of Test for Soils for Civil Engineering Purposes—Part 7: Shear Strength Tests (Total Stress)*; British Standards Institution: London, UK, 1990.
23. Bureau of Indian Standards (BIS). *IS 2720 (Part 13):1986: Methods of Test for Soils—Part 13: Direct Shear Test*; Bureau of Indian Standards: New Delhi, India, 1986.
24. Stacho, J.; Sulovska, M. Shear Strength Properties of Coarse-Grained Soils Determined Using Large-Size Direct Shear Test. *Civ. Environ. Eng.* **2022**, *18*, 244–257. https://doi.org/10.2478/cee-2022-0023.
25. Tiwari, B.; Brandon, T.L.; Marui, H.; et al. Comparison of Residual Shear Strengths from Back Analysis and Ring Shear Tests on Undisturbed and Remolded Specimens. *J. Geotech. Geoenviron. Eng.* **2005**, *131*, 1071–1079. https://doi.org/10.1061/(asce)1090-0241(2005)131:9(1071).
26. de Alba, P.; Ballestero, T.P. Residual strength after liquefaction: A rheological approach. *Soil Dyn. Earthq. Eng.* **2006**, *26*, 143–151. https://doi.org/10.1016/j.soildyn.2005.02.011.
27. Dong, Q.; Zhou, Z.; Li, X.; et al. Soil dynamic constitutive model considering post-liquefaction deformation and reversible pore-water pressure. *Sustainability* **2022**, *14*, 16512. https://doi.org/10.3390/su142416512.
28. Sarı, S.B. Probability-Based Assessment of Post-Liquefaction Shear Strength: An Effective Stress Approach. Master's Thesis, Middle East Technical University, Ankara, Türkiye, 2022.
29. Seed, H.B.; Idriss, I.M. Simplified Procedure for Evaluating Soil Liquefaction Potential. *J. Soil Mech. Found. Div.* **1971**, *97*, 1249–1273. https://doi.org/10.1061/jsfeaq.0001662.
30. Sett, S.; Chattopadhyay, K.K.; Ghosh, A. Liquefaction hazard mapping and relationship between probability of liquefaction and factor of safety for Kolkata city, India. *Nat. Hazards* **2023**, *118*, 347–376. https://doi.org/10.1007/s11069-023-06007-9.
31. Boulanger, R.W.; Idriss, I.M. *Evaluating the Potential for Liquefaction or Cyclic Failure of Silts and Clays*; Report No. UCD/CGM-04/01; University of California: Davis, CA, USA, 2004.
32. Padmanabhan, G.; Maheshwari, B.K. Reliquefaction resistance of Solani sand subjected to repeated excitations using shaking table experiments. *Bull. Earthq. Eng.* **2024**, *22*, 4797–4822. https://doi.org/10.1007/s10518-024-01937-6.
33. Afrazi, M.; Yazdani, M. Determination of the Effect of Soil Particle Size Distribution on the Shear Behavior of Sand. *J. Adv. Eng. Comput.* **2021**, *5*, 125–134. https://doi.org/10.25073/jaec.202152.331.
34. Baziar, M.H.; Dobry, R. Residual Strength and Large-Deformation Potential of Loose Silty Sands. *J. Geotech. Eng.* **1995**, *121*, 896–906. https://doi.org/10.1061/(asce)0733-9410(1995)121:12(896).
35. Bureau of Indian Standards (BIS). *IS 2720 (Part 14):1983: Methods of Test for Soils—Part 14: Determination of Density Index (Relative Density) of Cohesionless Soils*; Bureau of Indian Standards: New Delhi, India, 1983.
36. Bureau of Indian Standards (BIS). *IS 2720 (Part 28):1974: Methods of Test for Soils—Part 28: Determination of Dry Density of Soils, In-Place, by the Sand Replacement Method; Bureau of Indian Standards*: Bureau of Indian Standards: New Delhi, India, 1974.
37. Gates, I.D. Post-Liquefaction Residual Strength of Saturated and Partially Saturated Soils. Master's Thesis, University of New Hampshire, Durham, NH, USA, 2021.

38. Krim, A.; Arab, A.; Chemam, M.; et al. Experimental study on the liquefaction resistance of sand–clay mixtures: Effect of clay content and grading characteristics. *Mar. Georesources Geotechnol.* **2019**, *37*, 129–141. https://doi.org/10.1080/1064119x.2017.1407974.
39. Mohanty, B.; Kumar, P.; Patra, N.; et al. Evaluation of residual strength and liquefaction potential of pond ash. *Int. J. Geotech. Eng.* **2010**, *4*, 483–493. https://doi.org/10.3328/ijge.2010.04.04.483-493.
40. Mohammadi, M.; Fatemi Aghda, S.M.; Talkhablou, M.; et al. Prediction of the shear strength parameters from easily-available soil properties by means of multivariate regression and artificial neural network methods. *Geomech. Geoengin.* **2022**, *17*, 442–454. https://doi.org/10.1080/17486025.2020.1778194.
41. Bouaricha, L.; Khatti, J.; Yazici, M.F.; et al. Effect of polypropylene fiber, moisture content, relative density, and vertical stresses on mechanical properties of poorly graded sandy soil: A geotechnical and hybrid XGBoost-based investigation. *Constr. Build. Mater.* **2025**, *493*, 143286. https://doi.org/10.1016/j.conbuildmat.2025.143286.
42. Khatti, J.; Bouaricha, L.; Denine, S. Data-Driven Modeling of Strength Properties in Waste-Stabilized Soils: A Review of Artificial Intelligence Approaches. In *Intelligent Predictive Systems: AI and Machine Learning in Engineering*; Springer Nature Singapore: Singapore, 2026; pp. 129–150. https://doi.org/10.1007/978-981-95-7766-8_6.
43. Bureau of Indian Standards (BIS). *IS 1498:1970: Classification and Identification of Soils for General Engineering Purpose*, 1st ed.; Bureau of Indian Standards: New Delhi, India, 1970.
44. Afrazi, M.; Armaghani, D.J.; Afrazi, H.; et al. Geotechnical implications of sand–rubber mixture in transportation infrastructure: Assessing shear strength and compressibility characteristics. *Innov. Infrastruct. Solut.* **2025**, *10*, 403. https://doi.org/10.1007/s41062-025-02173-w.